Ferromagnetic resonance evidence for long-range ferromagnetic ordering in amorphous Fe-rich $Fe_{100-x}Zr_x$ alloys

1992 J. Phys.: Condens. Matter 4 505

(http://iopscience.iop.org/0953-8984/4/2/018)

J. Phys.: Condens. Matter 4 (1992) 505–524. Printed in the UK

Ferromagnetic resonance evidence for long-range ferromagnetic ordering in amorphous Fe-rich $Fe_{100-x}Zr_x$ alloys

S N Kaul and V Siruguri
School of Physics, University of Hyderabad, Central University PO, Hyderabad 500 134, India

Received 15 August 1990, in final form 4 July 1991

Abstract. Ferromagnetic resonance (FMR) measurements have been performed on amorphous (a-) $Fe_{100-x}Zr_x$ alloys with $x = 9$ and 10 and on a-$Co_{90}Zr_{10}$ for horizontal–perpendicular, horizontal–parallel and vertical–parallel sample geometries at a fixed microwave frequency of about 9.3 GHz in the temperature range 77 to 500 K. In the horizontal–parallel ($\|^h$) and vertical–parallel ($\|^v$) orientations, the peak-to-peak FMR linewidth (ΔH_{pp}) remains constant at a value of about 210 Oe (290 Oe) for $Fe_{90}Zr_{10}$($Fe_{91}Zr_9$) in the temperature range 115 K $\leqslant T \leqslant 0.8T_C$ (Curie temperature), while the resonance field (H_{res}) as a function of temperature increases slowly up to $0.8T_C$ and for $T > 0.8T_C$ both ΔH_{pp} and H_{res} start increasing at a rapid rate. Values of the 'in-plane' uniaxial anisotropy field, H_k, and Gilbert damping parameter, λ, at different temperatures $T \leqslant T_C$ determined from the observed values of $H_{res}^{\|^v}$, $H_{res}^{\|^h}$ and $\Delta H_{pp}^{\|^v}$, $\Delta H_{pp}^{\|^h}$ demonstrate that H_k and λ both scale with saturation magnetization, M_s. The temperature dependence of M_s deduced from the FMR results conforms very well with that previously observed by us for the bulk magnetization. At $T \geqslant T_C$, a secondary resonance, whose width goes through a minimum while the resonance field increases as the temperature is increased from $T = T_C$ to 500 K and for which $H_k = 0$, appears at low fields for the alloys with $x = 9$ and 10. The FMR data taken in the perpendicular geometry are consistent with those obtained for $\|^h$ and $\|^v$ configurations. By contrast, regardless of the sample geometry used, ΔH_{pp} remains constant whereas H_{res} exhibits a very weak dependence on temperature in the investigated temperature range (77 $\leqslant T \leqslant$ 500 K) for a-$Co_{90}Zr_{10}$. The present results have been discussed in light of the existing theories.

1. Introduction

Amorphous (a-) $Fe_{90\pm x}Zr_{10\mp x}$ ($0 \leqslant x \leqslant 3$) alloys have attracted considerable attention during recent years because they offer a rare possibility of investigating a unique combination of widely different but interesting physical phenomena (Kaul 1983). The magnetic phase diagram, based on bulk magnetization, Mössbauer and AC susceptibility data (Hiroyoshi and Fukamichi 1982, Kaul 1983, Saito *et al* 1986, Ryan *et al* 1987, Coey *et al* 1987), indicates a transition from the paramagnetic (PM) to the *ferromagnetic-like* (FM) state at the Curie temperature, T_C (T_C decreases with increasing Fe concentration), followed, at a lower temperature T_{SG} (T_{SG} increases as Fe concentration increases), by

0953-8984/92/020505 + 20 $04.50

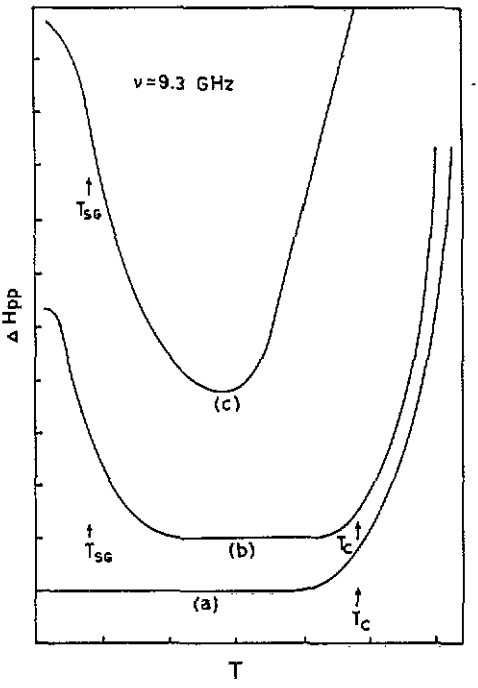

Figure 1. Schematic depiction of the typical variation of ΔH_{pp} with temperature normally observed in (*a*) conventional ferromagnets, (*b*) re-entrant spin-glass systems and (*c*) spin (or cluster spin) glasses.

another transition from the FM to the *spin-glass-like* (SG) state; the PM–FM and FM–SG transition lines meet at ≈93 at.% Fe. Intense experimental efforts devoted to the study of properties that characterize the FM and SG phases have so far failed to resolve the controversy surrounding the exact nature of these phases. For instance, the FM state has found two main but contradictory descriptions based on different experimental findings. On the one hand, the following observations have been made: (i) a low value of the saturation Fe atomic moment; (ii) a broad hyperfine field distribution with finite probability even at zero field (Oshima *et al* 1981, Yamamoto *et al* 1983, Tange *et al* 1986, Heller *et al* 1986, Ryan *et al* 1987, Coey *et al* 1987) for $T < T_C$; (iii) magnetic broadening (Ryan *et al* 1987, Coey *et al* 1987) in the Mössbauer spectra for temperatures well above T_C; (iv) values of the critical exponents considerably larger than those theoretically predicted for an ordered three-dimensional (3D) nearest-neighbour isotropic Heisenberg ferromagnet, which either satisfy (Winschuh and Rosenberg 1987) or do not satisfy (Yamauchi *et al* 1984) the Widom scaling relation; and (v) the *finite* (≈27 Å) spin–spin correlation length, ξ, at $T = T_C$ indicated by the small-angle neutron scattering (SANS) data (Rhyne and Fish 1985) on a-$Fe_{91}Zr_9$. Observations (i)–(v) have been taken to imply that the alloys in question behave either as 'wandering-axis ferromagnets', in which the spin structure is *locally ferromagnetic* (Ryan *et al* 1987, Coey *et al* 1987) with small variations in spin directions on neighbouring sites but the local ferromagnetic axis changes direction over distances of order ξ, or as a strongly exchange-frustrated system (Fish and Rhyne 1987) in which the *ferromagnetic correlations are short-ranged* (≈27 Å), or else these alloys enter the spin-glass state directly (Rhyne and Fish 1985) at $T = T_C$ (i.e. *in no case does a long-range ferromagnetic order develop at any temperature* and the transition at T_C is *not* a true phase transition in the thermodynamic sense). On the other

hand, AC susceptibility, χ_{ac}, measured in the absence and presence of a superposed static magnetic field (Kaul *et al* 1986, Kaul 1987, 1988) as well as the recent bulk magnetization, M, data (Kaul 1988, Reisser *et al* 1988) taken in a narrow temperature range around T_C demonstrate that the transition at T_C, marked by the divergence (Saito *et al* 1986, Kaul *et al* 1986, Kaul 1987, 1988) in 'zero-field' susceptibility at that temperature (the Curie point), is a second-order magnetic phase transition characterized by 3D Heisenberg-like critical exponents and the *ferromagnetic order for temperatures below T_C has a long-range character* as inferred from the demagnetization-limited behaviour of both $\chi_{ac}(T)$ and $M(T)$ in external DC fields $\leqslant$10 Oe for $T \leqslant T_C$. So far as the transition at T_{SG} is concerned, conflicting experimental observations (for details see Ghafari *et al* 1988), which either support (Hiroyoshi and Fukamichi 1982, Kaul 1983, Saito *et al* 1986, Ryan *et al* 1987, Coey *et al* 1987, Ghafari *et al* 1988) or refute (Beck and Kronmüller 1985, Read *et al* 1986) the existence of a re-entrant spin-glass phase at low temperatures and hence the occurrence of a transition to such a state at T_{SG}, have been reported. Considering the fact that the low-temperature magnetic phase and the transition at T_{SG} are bound to evade correct description so long as a complete knowledge about the transition at T_C is lacking, deeper physical insight into the high-temperature magnetic phase than gained hitherto becomes imperative. The present investigation, therefore, aims at unravelling the nature of magnetic order that exists for temperatures well above T_{SG} but below T_C.

In this paper, we report the results of the first detailed ferromagnetic resonance (FMR) measurements on amorphous (a-) $Fe_{90+x}Zr_{10-x}$ alloys with $x = 0$ and 1 and on a-$Co_{90}Zr_{10}$ in the temperature range 77 to 500 K. Suitability of the FMR technique for the type of study intended is dictated by its capability to distinguish clearly between different kinds of magnetic order because they give rise to markedly different variations of the FMR linewidth, Γ, with temperature. To elucidate this point further, Γ *stays constant* (Heinrich *et al* 1984) *at a low value* ($\simeq$100 *Oe*) *for* $T \leqslant 0.8T_C$ but increases steeply for temperatures above T_C (figure 1(*a*)) in the case of a concentrated 'homogeneous' amorphous ferromagnet (note that the *local* magnetization varies from site to site even in the most concentrated amorphous ferromagnet as is evidenced by a sizable frequency-independent (Heinrich *et al* 1984, Bhagat *et al* 1985) contribution to Γ) whereas Γ in a re-entrant spin glass (Bhagat *et al* 1985) *increases exponentially* as temperature is lowered below $\sim 2T_{SG}$, goes through a *flat minimum* (typical value at the minimum $\simeq$ 200 Oe at the frequency of the microwave field $\nu = 9.3$ GHz) within the temperature interval $2T_{SG}$ ($\nu = 9.3$ GHz) $\leqslant T \leqslant 0.8T_C$ (the lower limit of this interval depends on ν) and exhibits a steep rise for $T > T_C$ (figure 1(*b*)). Contrasted with the afore-mentioned variations of Γ with T, Γ at $\nu \simeq 9.3$ GHz $\propto T\exp(-T/T_0)$ for $T \leqslant 3T_{SG}$ and passes through a broad minimum (typical value at the minimum $\simeq$ 500 Oe) around $3T_{SG}$ before displaying a linear dependence on temperature (in the paramagnetic region) for an amorphous cluster spin glass (mictomagnet) with composition just below the percolation threshold (Park *et al* 1986) (figure 1(*c*)). A comprehensive study of the temperature dependence of FMR linewidth carried out presently, therefore, provides for the first time *unambiguous* evidence for the existence of a *long-range inhomogeneous ferromagnetic order* for temperatures in the range 77 K $\leqslant T \leqslant T_C$. Furthermore, of all the model descriptions for the type of magnetic order present in these glassy alloys proposed hitherto, our results favour a model (Kaul 1984, 1985, Kaul *et al* 1986, Kaul 1987, 1988, 1991) that postulates the spin system for $T \leqslant T_C$ to consist of the *infinite three-dimensional ferromagnetic* (*FM*) *cluster* (which forms the FM network or matrix) and *finite spin clusters* (the spins within these clusters are also *ferromagnetically* coupled) embedded in, but 'isolated' from, this FM matrix.

2. Experimental details

Amorphous $Fe_{90}Zr_{10}$, $Fe_{91}Zr_9$ and $Co_{90}Zr_{10}$ alloys were prepared under helium (inert) atmosphere by a melt-spinning technique in the form of long ribbons of ~2 mm width and 30–40 μm thickness. X-ray diffractometric and electron microscopic examination of both the dull and shiny sides of the ribbons so fabricated revealed no traces of either surface crystallization or a second minor crystallographic phase and provided no evidence for amorphous phase separation. After confirming that the atomic arrangement in these ribbons corresponds to an amorphous 'single-phase' state, the field derivative of the microwave power (P) absorbed during the ferromagnetic resonance (FMR) process, dP/dH, was measured as a function of the external static magnetic field (H) on 4 mm long strips, cut from the alloy ribbons, using horizontal–parallel ($\|^h$), vertical–parallel ($\|^v$) and horizontal–perpendicular ($\perp^h$) sample configurations, at a fixed microwave field frequency of $\simeq$9.25 GHz on a JEOL FE-3X EPR spectrometer in the temperature range 77 to 500 K. In the $\|^h$ ($\|^v$) sample geometry, H lies in the ribbon plane and is directed along the length (breadth), whereas in the $\perp^h$ geometry H is normal to the ribbon plane; the $\|^h$ sample geometry transforms into the $\perp^h$ configuration when the ribbon strip is rotated by 90° about an axis that lies in the ribbon plane and is directed along the breadth while keeping the direction of H fixed. The temperature was measured by a precalibrated copper–constantan thermocouple situated just outside the microwave cavity a few centimetres away from the sample and was held constant to within $\pm$0.1 K at every temperature setting by regulating the flow of cold nitrogen gas around the sample by controlling the power input to the heater, immersed in a container filled with liquid nitrogen, with the aid of a PID temperature controller. The actual sample temperature was then determined from the temperature T^* so measured by correcting T^* using the results of a separate empty cavity run in which the measuring thermocouple was calibrated against another (precalibrated) copper–constantan thermocouple situated at the sample site. Curves of dP/dH against H at 77 K were recorded for the sample configurations mentioned above by mounting the sample into the quartz tail, contained within the cavity, of the glass dewar full of liquid nitrogen such that the sample is at the centre of the cavity. Highly precise and reproducible data free from specious stress-induced effects were obtained by making an appropriate choice (Mohan Babu 1988, Kaul and Mohan Babu 1989) of the sample mounting technique. Data taken on strips cut from different parts of the alloy ribbon and on the same alloy strip remounted several times established that the resonance field and the peak-to-peak FMR linewidth are reproduced to within $\pm$2% and $\pm$10%, respectively.

3. Results and data analysis

Figure 2 depicts the observed functional dependence of dP/dH on H in the horizontal–parallel ($\|^h$) configuration at a few selected values of temperature for a-$Fe_{90}Zr_{10}$. The power absorption derivative (PAD) curves displayed in this figure are also representative of those recorded for a-$Fe_{90}Zr_{10}$ in the vertical–parallel ($\|^v$) sample configuration and for $Fe_{91}Zr_9$ in both $\|^h$ and $\|^v$ sample geometries. Resonance field, H_{res} (defined as the field where the $dP/dH = 0$ line cuts the dP/dH versus H curve or alternatively as the field where dP/dH possesses half the peak-to-peak value if the dP/dH versus H curve is symmetrical about the baseline), and 'peak-to-peak' linewidth, ΔH_{pp}, deduced from the PAD curves for both $\|^h$ and $\|^v$ configurations, as functions of temperature are depicted in

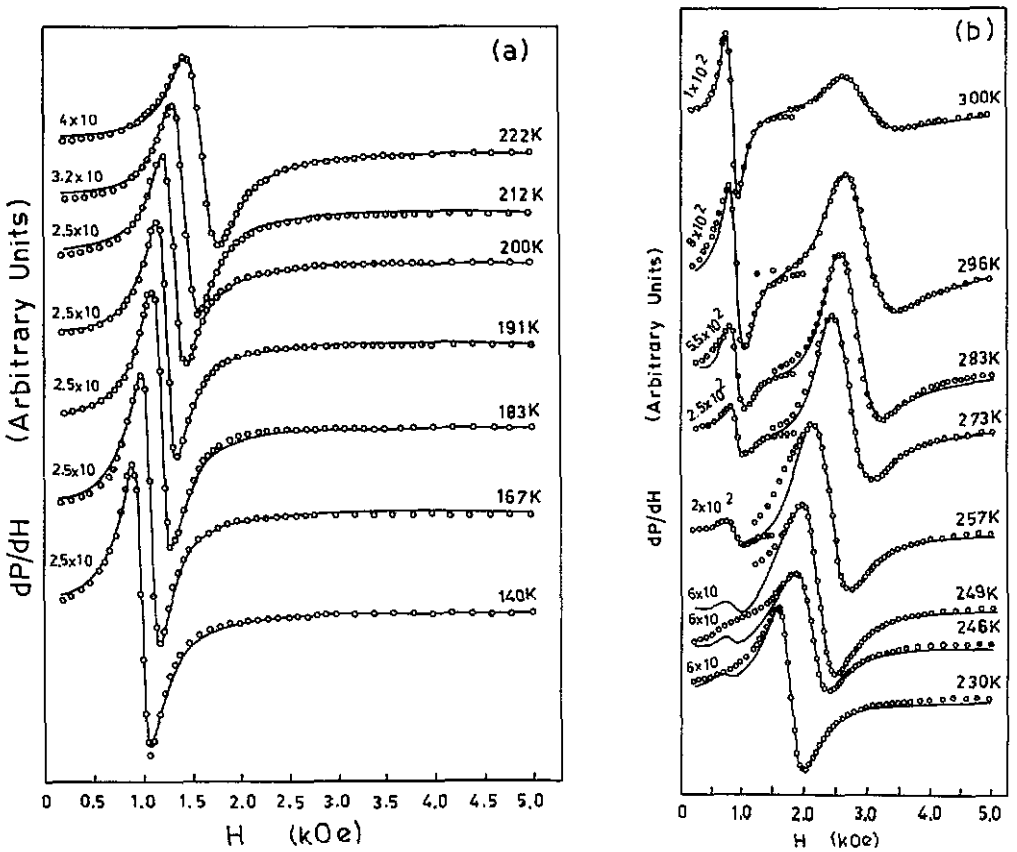

Figure 2. Field dependence of the microwave power absorption derivatives for a-$Fe_{90}Zr_{10}$ at a few representative fixed temperature values lying below and above the Curie temperature, T_C, using horizontal–parallel sample geometry. Full curves depict the observed variation whereas the open circles denote the values calculated using equations (1) and (2) of the text. Numbers on the left-hand side of the curves denote the sensitivity at which the spectra are taken.

figures 3–6 for amorphous $Fe_{90}Zr_{10}$ and $Fe_{91}Zr_9$ alloys. For a-$Fe_{90}Zr_{10}$ (a-$Fe_{91}Zr_9$)† alloy, H_{res} exhibits a slow increase up to $T_C = 240 \pm 1$ K ($T_C = 212 \pm 1$ K), determined from bulk magnetization (Kaul 1983) (AC susceptibility (Kaul *et al* 1986)) measurements, whereas ΔH_{pp} goes through a flat minimum in the temperature range $0.5T_C \lesssim T \lesssim 0.8T_C$ ($0.6T_C \lesssim T \lesssim 0.8T_C$) where it assumes a constant (within error limits) value $\simeq 210$ Oe ($\simeq 290$ Oe) for both $\|^h$ and $\|^v$ orientations. The broken curves in figure 5 depict the variation of ΔH_{pp} with temperature at low temperatures obtained from the expression (Bhagat *et al* 1985)

$$\Delta H_{pp} = \Gamma_0 + \Gamma_1(T/T_0)\exp(-T/T_0)$$

with the choice of the parameters $\Gamma_0 = 190$ Oe (281 Oe), $\Gamma_1 = 6100$ Oe (8266 Oe) and

† Values of quantities within parentheses henceforth refer to a-$Fe_{91}Zr_9$.

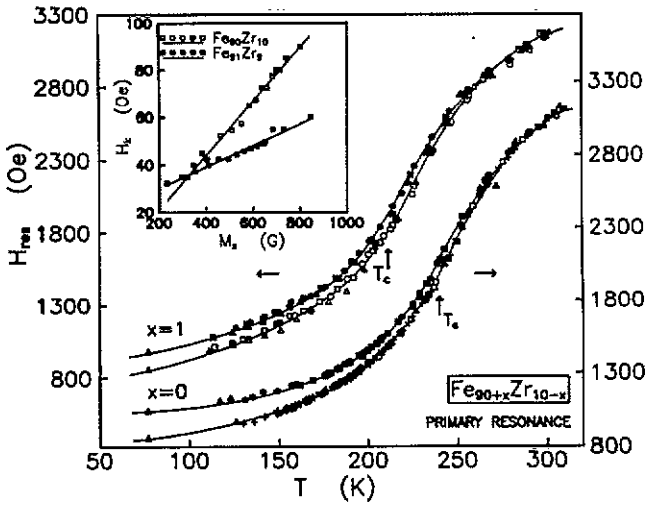

Figure 3. Temperature dependence of the resonance field, H_{res}, for the primary resonance in $Fe_{90}Zr_{10}$ and $Fe_{91}Zr_9$ amorphous alloys. Open and full symbols denote the experimental data taken using the horizontal–parallel and vertical–parallel sample configurations, respectively; □, ■, ☆, ◇, ○, ●, ×, + represent the data taken in different experimental runs on sample 1 whereas △, ▲ denote data taken in a single experimental run on sample 2. In the case of a-$Fe_{91}Zr_9$, however, ○, ● denote the data taken on sample 3 instead of sample 1. The inset shows H_k plotted against M_s.

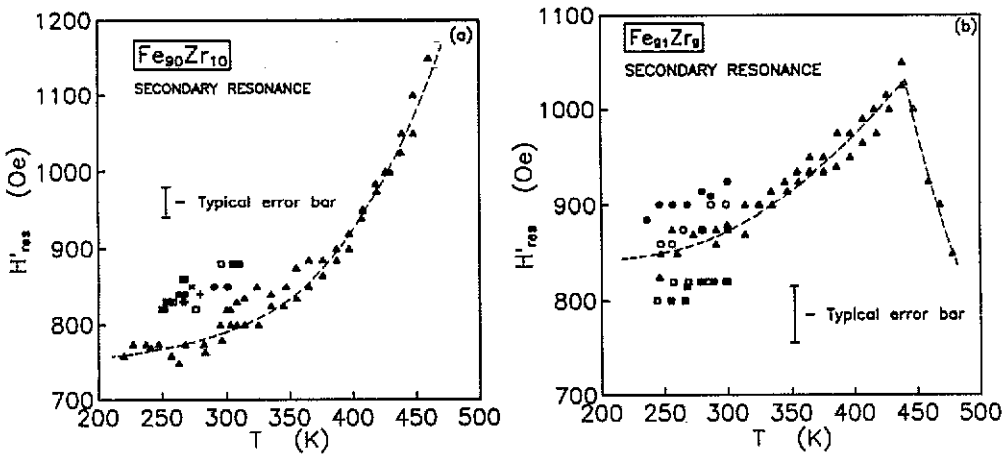

Figure 4. Temperature dependence of the resonance field, H'_{res}, for the secondary resonance in (*a*) $Fe_{90}Zr_{10}$ and (*b*) $Fe_{91}Zr_9$. Data symbols represent the same experimental runs as in figure 3. The broken curves through the data points serve to illustrate the observed trend.

$T_0 = 16.7$ K (17.0 K) for a-$Fe_{90}Zr_{10}$ (a-$Fe_{91}Zr_9$). Apart from this resonance (henceforth referred to as the primary or main resonance), which not only shifts to higher fields but also broadens out at a rapid rate as the temperature is increased beyond T_C (figures 3 and 5), the signature of a secondary resonance at a lower field value, i.e.

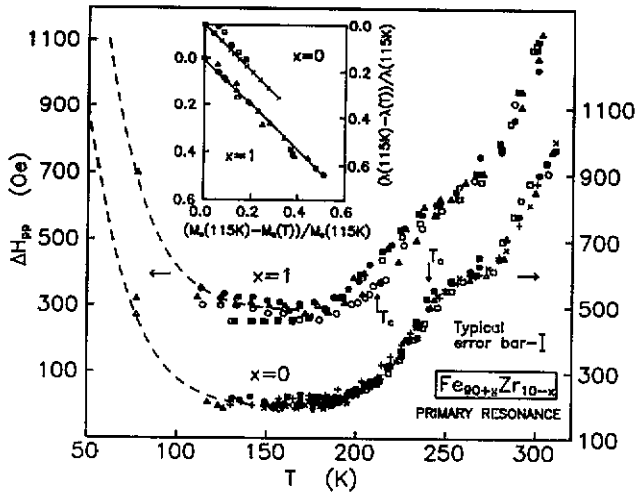

Figure 5. Variation with temperature of the peak-to-peak linewidth, ΔH_{pp}, for the primary resonance in $Fe_{90}Zr_{10}$ and $Fe_{91}Zr_9$ amorphous alloys. The inset shows the reduced λ versus reduced M_s plots for the two alloys. Data symbols have the same meaning as for figure 3.

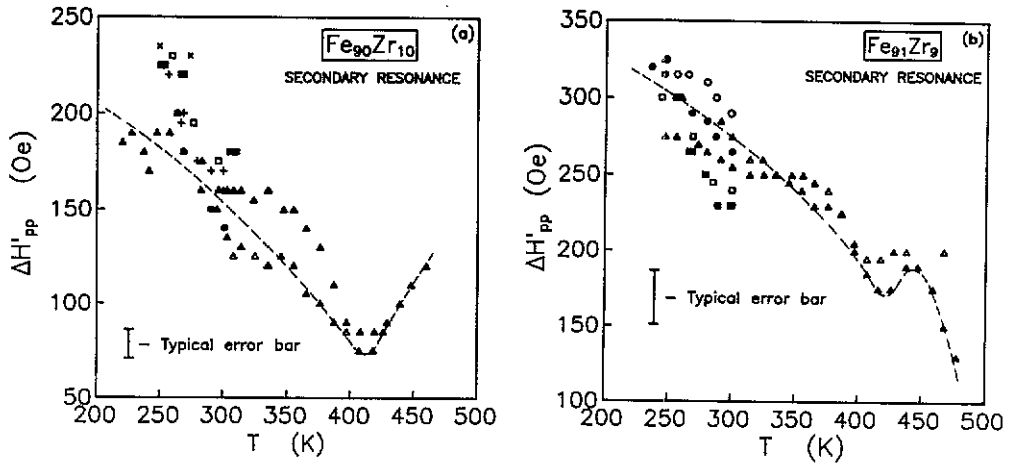

Figure 6. Variation of $\Delta H'_{pp}$ with temperature for the secondary resonance in the case of (*a*) $Fe_{90}Zr_{10}$ and (*b*) $Fe_{91}Zr_9$. Data symbols represent the same experimental runs as in figure 3. The broken curves through the data points serve to illustrate the observed trend.

$H'^{(\|h)}_{res} = H'^{(\|v)}_{res} \simeq 800$ Oe ($\simeq$850 Oe) is first noticed at $T \simeq T_C$ in the most sensitive setting of the spectrometer (figure 2(*b*)). The appearance of the secondary resonance is associated with a slope change in the ΔH_{pp} versus T curve (figure 5) but this resonance can be resolved better only for temperatures in excess of $T_C + 10$ K. H'_{res} increases while $\Delta H'_{pp}$ goes through a minimum at $T_{min} \simeq 410$ K within the temperature interval $T_C + 10\,\text{K} \leqslant T \leqslant 500$ K (an additional feature of the data in the case of a-$Fe_{91}Zr_9$ is a steep decline in both H'_{res} and $\Delta H'_{pp}$ for $T \geqslant 450$ K). In order to ascertain whether or not the observed resonances (both primary and secondary) are characteristic of the bulk, a series of etching and mechanical polishing experiments were performed (Siruguri

et al 1991) in which PAD curves were recorded at a few representative temperatures including room temperature on samples etched in 10% HNO_3 plus 90% ethanol solution for various lengths of time and on samples that had been mechanically polished before and after etching. These experiments unambiguously demonstrate that both the primary and secondary resonances originate from the bulk and not from the surface. The finding that ΔH_{pp} forms a sizable fraction of H_{res} ($\Delta H_{pp}/H_{res} \simeq 0.2$ (0.25) at $T =$ 115 K and $\Delta H_{pp}/H_{res} \simeq 0.30$ (0.34) at $T = 300$ K for the primary resonance whereas $\Delta H'_{pp}/H'_{res} \simeq 0.24$ (0.30) for the secondary resonance in the temperature range $T_C + 10$ K to 300 K) necessitates a complete lineshape calculation for each resonance line separately because the observed value of H_{res} can differ significantly from the actual ('true') resonance centre due to appreciably large linewidth. Therefore, the least-squares fits to the observed dP/dH versus H curves have been attempted based on the theoretical expression (Kaul and Siruguri 1987) derived for the parallel geometry used in this work, i.e.

$$\frac{dP_{\parallel}}{dH} \propto \frac{d}{dH}[(\mu'^2 + \mu''^2)^{1/2} + \mu'']^{1/2} \tag{1}$$

with the real and imaginary components of the dynamic permeability given by (see appendix)

$$\mu' = \{[(H + H_k)(B + H_k) - \Gamma^2 - (\omega/\gamma)^2][(B + H_k)^2 - \Gamma^2 - (\omega/\gamma)^2] + 2\Gamma^2(B + H_k)(B + H + 2H_k)\}\{[(H + H_k)(B + H_k) - \Gamma^2 - (\omega/\gamma)^2]^2 + \Gamma^2(B + H + 2H_k)^2\}^{-1} \tag{2a}$$

$$\mu'' = \{-2\Gamma(B + H_k)[(H + H_k)(B + H_k) - \Gamma^2 - (\omega/\gamma)^2] + \Gamma(B + H + 2H_k)[(B + H_k)^2 - \Gamma^2 - (\omega/\gamma)^2]\} \times \{[(H + H_k)(B + H_k) - \Gamma^2 - (\omega/\gamma)^2]^2 + \Gamma^2(B + H + 2H_k)^2\}^{-1} \tag{2b}$$

where the most energetically favourable orientation of the magnetization vector in zero external magnetic field dictated by both shape anisotropy and 'in-plane' uniaxial anisotropy is assumed to be along the length in the ribbon plane, $B = H + 4\pi M_s$, M_s is the saturation magnetization, H_k is the 'in-plane' uniaxial anisotropy field, $\nu = \omega/2\pi$ is the frequency of the microwave field, $\gamma = g|e|/2mc$ is the magnetomechanical ratio, $\Gamma = \lambda\omega/\gamma^2 M_s$ is the linewidth parameter and λ is the Gilbert damping parameter, by making use of a non-linear least-squares-fit computer program which treats the Landé splitting factor g and $4\pi M_s$ as free fitting parameters while using the observed values of $\Delta H_{pp} = 1.45\Gamma$ and the values of H_k derived from the following relations† (see appendix)

$$H_{res}^{\parallel h} = H_{res}^{\parallel} - H_k \tag{3a}$$

and

$$H_{res}^{\parallel v} = H_{res}^{\parallel} + H_k. \tag{3b}$$

In equations (3*a*) and (3*b*), $H_{res}^{\parallel h}$ and $H_{res}^{\parallel v}$ are the resonance fields observed in the

† Note that the relations (3*a*) and (3*b*) are consistent not only with (4*a*) and (4*b*) but also with the observation that the resonance field as a function of the angle θ between the external static field direction and length *in the ribbon plane* goes through a minimum at $\theta = 0°$ ($\parallel^h$ configuration) and a maximum at $\theta = 90°$ ($\parallel^v$ configuration).

horizontal– and vertical–parallel orientations, respectively, and $H^{\parallel}_{res}$ is the resonance field in the absence of H_k defined by the relation

$$(\omega/\gamma)^2 + \Gamma_{\parallel}^2 = H^{\parallel}_{res}(H^{\parallel}_{res} + 4\pi M_s).$$

Theoretical fits so obtained are denoted by open circles in figure 2. The main findings, based on the data presented in figures 2–6 and the lineshape analysis, are: (i) H_k *scales with* M_s for the *main resonance* for $T \leqslant T_C$ (inset of figure 3); (ii) by contrast, $H_k = 0$ (i.e. $H'^{\parallel h}_{res} = H'^{\parallel v}_{res}$ within the uncertainty limits) for the *secondary resonance* even though M_s *has a considerably large value*, which decreases as the temperature is increased from $(T_C + 10\ K)$ to 450 K; (iii) $\lambda \propto M_s$ (inset of figure 5) for the *primary resonance* within the temperature region $115\ K \leqslant T \leqslant 0.8T_C$ where ΔH_{pp} remains constant; (iv) *FMR linewidth possesses the same value* (within the error limits) *regardless* of the orientation of H in the ribbon plane and g has a *temperature-independent* value of $g = 2.07 \pm 0.02$ for *both primary and secondary resonances*; and (v) corrections to the observed values of H_{res} due to finite linewidth turn out to be negligibly small even for the main resonance for temperatures as high as 325 K where ΔH_{pp} attains a fairly large value. The last result is consistent with the observation that the experimental values of $H^{\parallel h}_{res}$ and $H^{\parallel v}_{res}$ satisfy the resonance conditions (see appendix for details)

$$[(\omega/\gamma)^2 + \Gamma^2_{\parallel h}] = (H^{\parallel h}_{res} + 4\pi M_s + H_k)(H^{\parallel h}_{res} + H_k) \tag{4a}$$

and

$$[(\omega/\gamma)^2 + \Gamma^2_{\parallel v}] = (H^{\parallel v}_{res} + 4\pi M_s - H_k)(H^{\parallel v}_{res} - H_k) \tag{4b}$$

obtained by solving the Landau–Lifshitz–Gilbert (LLG) phenomenological equation of motion for dynamic magnetization

$$\frac{d\boldsymbol{M}}{dt} = -\gamma(\boldsymbol{M} \times \boldsymbol{H}_{eff}) + \frac{\lambda}{\gamma M_s^2}\left(\boldsymbol{M} \times \frac{d\boldsymbol{M}}{dt}\right) \tag{5}$$

for the sample geometries in question. In equation (5), $\boldsymbol{H}_{eff}$ is the effective magnetic field (Kaul and Siruguri 1987) 'seen' by the spins. Note that the exchange term $(2A\gamma/M^2)(\boldsymbol{M} \times \nabla^2\boldsymbol{M})$ in equation (5) has been dropped in view of the observation (Bhagat *et al* 1977, Kaul and Srinivasa Kasyapa 1989) that the contributions due to this term to the linewidth and resonance field are so small as to fall well within the error limits because the macroscopic exchange stiffness parameter, A, and conductivity are both at least an order of magnitude lower (Kaul 1983, Beck and Kronmüller 1985, Kaul *et al* 1991) than their corresponding values for crystalline metals. Moreover, the values of the parameters g and $4\pi M_s$ [H_k] determined from the lineshape analysis (equation (3)) of the data taken in the $\parallel$ geometry for the main resonance on amorphous $Fe_{90}Zr_{10}$ and $Fe_{91}Zr_9$ alloys and the observed values of $\Gamma_\perp$ when used in the expression (appendix)

$$[(\omega/\gamma)^2 + \Gamma^2_{\perp}] = (H^{\perp h}_{res} - 4\pi M_s - H_k)(H^{\perp h}_{res} - 4\pi M_s) \tag{6}$$

to derive the values of H_{res} for the horizontal–perpendicular ($\perp^h$) orientation yield values for $H^{\perp h}_{res}$ that exactly coincide with the experimentally observed values for $T \geqslant T_C$. However, in the temperature ranges $77\ K \leqslant T \leqslant T_C$ for the primary resonance and $(T_C + 10\ K) \leqslant T \leqslant 500\ K$ for the secondary resonance, $4\pi M_s$ is substantially large so that the resonance in the $\perp^h$ configuration occurs at fields higher than 10 kOe, the upper instrumental limit. Therefore, in the $\perp^h$ geometry, the secondary resonance is not observed at any temperature whereas the primary resonance is detected for $T > T_C$ only.

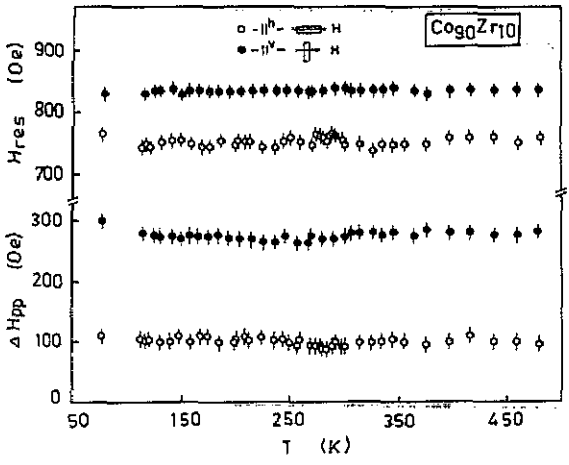

Figure 7. Resonance field, H_{res}, and peak-to-peak linewidth, ΔH_{pp}, for horizontal–parallel ($\|^h$) and vertical–parallel ($\|^v$) sample geometries as functions of temperature for a-$Co_{90}Zr_{10}$.

In order to gain further physical insight into the nature of magnetism in Fe-rich Fe–Zr amorphous alloys for temperatures near the upper transition temperature, a detailed comparative FMR study on a-$Co_{90}Zr_{10}$ alloy, which is known (Kaul 1983) to exhibit conventional ferromagnetism down to 4.2 K, was undertaken. In contrast with the temperature-induced variations in the parameters H_{res}, ΔH_{pp}, $4\pi M_s$, λ and H_k for the main resonance in a-$Fe_{90}Zr_{10}$ and a-$Fe_{91}Zr_9$ alloys, the quantities $\Delta H_{pp}^{\|h} = 100 \pm 10$ Oe, $\Delta H_{pp}^{\|v} = 290 \pm 10$ Oe and $g = 2.09 \pm 0.02$ remain unaltered (within error limits) while $H_{res}^{\|h}$ and $H_{res}^{\|v}$ (hence M_s, H_k and λ) have a slight but finite variation with temperature for a-$Co_{90}Zr_{10}$ in the temperature range covered in the present experiments (figure 7), as expected for a ferromagnet with a high Curie temperature ($T_C > 700$ K (Tange *et al* 1986) for a-$Co_{90}Zr_{10}$). However, as in the case of former glassy alloys, both H_k and λ scale with M_s for a-$Co_{90}Zr_{10}$ too.

4. Discussion

The finding that the 'in-plane' uniaxial anisotropy field, $H_k = (2K_u/M_s)$, is related to the saturation magnetization, M_s, through a *linear* relation of the type $H_k(T) = \alpha M_s(T)$, or alternatively $K_u(T) = (\alpha/2)[M_s(T)]^2$, indicates that the coupling energy of the anisotropy is dipolar in origin, i.e. this anisotropy probably results from the atomic pair ordering (Hasegawa 1975, 1983, Fujimori 1983) which may be introduced during the rapid solidification process. Slope α, determined by the least-squares-fit method (inset of figure 3), yields values of the uniaxial anisotropy constant K_u at $T = 77$ K for a-$Fe_{90}Zr_{10}$ and a-$Fe_{91}Zr_9$ alloys as K_u (77 K) $= (2.91 \pm 0.40) \times 10^4$ erg cm^{-3} and $(1.6 \pm 0.2) \times 10^4$ erg cm^{-3}, respectively. These values are *typical* (Hasegawa 1975, Hasegawa *et al* 1976, Luborsky and Walter 1977, Takahashi and Kim 1978, Luborsky 1980, Fujimori 1983) of amorphous 3d transition metal (TM)–metalloid (M) alloys containing 78 to 85 at.% TM, which exhibit long-range ferromagnetism.

Before embarking upon a discussion of the parameters deduced from the lineshape analysis, a few remarks need to be made concerning the lineshape analysis itself. The equation of motion for the dynamic magnetization, equation (5), on which (1) and (2) are based, is strictly valid for a single-crystal ferromagnetic alloy in which magnetization

is uniform and $\boldsymbol{H}_{\rm eff} = \boldsymbol{H} + \boldsymbol{H}_{\rm int}$, where $\boldsymbol{H}$ is the static applied magnetic field and $\boldsymbol{H}_{\rm int} = \boldsymbol{H}_{\rm k} - \boldsymbol{H}_{\rm dem} + \boldsymbol{H}_{\rm an}$ includes the demagnetizing field, $\boldsymbol{H}_{\rm dem}$, $\boldsymbol{H}_{\rm k}$ and other anisotropy fields, $\boldsymbol{H}_{\rm an}$, with easy axis along $\boldsymbol{H}$. Detailed frequency-dependent FMR measurements (Kraus *et al* 1981, Heinrich *et al* 1984, Bhagat *et al* 1985) on a large number of amorphous ferromagnetic alloys have revealed that $\Delta H_{\rm pp}$ varies with the microwave field frequency, ν, as $(a + b\nu)$ in the temperature range where $\Delta H_{\rm pp}$ remains constant. While the term linear in ν has its origin in the LLG relaxation and hence can be adequately described by equation (5) provided $\boldsymbol{M}$ and $\boldsymbol{H}_{\rm int}$ are replaced by their average values, i.e. $\langle \boldsymbol{M} \rangle$ and $\langle \boldsymbol{H}_{\rm int} \rangle$, the constant term arises from exchange fluctuations, inhomogeneous magnetization and *local* random anisotropy (caused by the topological disorder) and can be accounted for either by using the fluctuating parts of $\boldsymbol{M}$ and $\boldsymbol{H}_{\rm int}$, i.e. $\delta\boldsymbol{M}(\boldsymbol{r}, t)$ and $\delta\boldsymbol{H}_{\rm int}(\boldsymbol{r}, t)$, instead of $\boldsymbol{M}$ and $\boldsymbol{H}_{\rm int}$ in equation (5) or by invoking two-magnon scattering mechanism (Heinrich *et al* 1985, Cochrane *et al* 1989). In other words, in the former approach, for amorphous ferromagnets, $\boldsymbol{M}$ and $\boldsymbol{H}_{\rm eff}$ in equation (5) should be replaced by $\boldsymbol{M} = \langle \boldsymbol{M} \rangle + \delta\boldsymbol{M}(\boldsymbol{r}, t)$ and $\boldsymbol{H}_{\rm eff} = \boldsymbol{H} + \boldsymbol{H}_{\rm int}(\boldsymbol{r}, t) = \boldsymbol{H} + [\langle \boldsymbol{H}_{\rm int} \rangle + \delta\boldsymbol{H}_{\rm int}(\boldsymbol{r}, t)]$. Following Bhagat *et al* (1977, 1985) and Heinrich *et al* (1984), the microwave power absorbed during the resonance process could then be calculated by assuming Gaussian distributions for magnetization and internal fields centred around $\langle M \rangle \equiv M_{\rm s}$ and $\langle H_{\rm int} \rangle$ with standard deviations δ_M and $\delta_{H_{\rm i}}$, respectively. It turns out that the inclusion of δ_M and $\delta_{H_{\rm i}}$ has only a slight (Bhagat *et al* 1985) effect on the lineshape but explains the increased magnitude of $\Delta H_{\rm pp}$. Consequently, it is possible to disregard the frequency- and temperature-independent contribution to $\Delta H_{\rm pp}$ and represent the resonance line by a $\lambda_{\rm eff}$ value in equation (5) but now $\lambda_{\rm eff}$ would be a function of ν. While performing the lineshape analysis of the observed FMR spectra, we have adopted the latter approach, which is noticed (figure 2) to reproduce very closely all the observed spectra for the glassy alloys in question including those taken at $T > T_{\rm C}$ and exhibiting marked asymmetry. Instead of relying on $\lambda_{\rm eff}$ values so obtained, which are bound to overestimate λ in the absence of a complete knowledge about the constant part of $\Delta H_{\rm pp}$, a direct relation between λ and $M_{\rm s}$ of the type $\lambda \propto M_{\rm s}$ within the temperature range where $\Delta H_{\rm pp}$ remains constant is clearly brought out by plotting the reduced Gilbert damping parameter, $[\lambda(115\ {\rm K}) - \lambda(T)]/\lambda(115\ {\rm K})$, against reduced magnetization, $[M_{\rm s}(115\ {\rm K}) - M_{\rm s}(T)]/M_{\rm s}(115\ {\rm K})$, in the inset of figure 5. The general observation that the property $\lambda \propto M_{\rm s}$ is *characteristic* (Bhagat *et al* 1977, Kaul and Siruguri 1987) of a wide variety of amorphous and crystalline ferromagnets then asserts that the main resonance in a-$Fe_{90}Zr_{10}$ and a-$Fe_{91}Zr_9$ alloys originates from the long-range ferromagnetic ordering of spins for $T < T_{\rm C}$. This claim is further substantiated by the fact that a comparison between the functional dependences of $\Delta H_{\rm pp}$ on T shown in figures 1 and 5 demonstrates that the variation of $\Delta H_{\rm pp}$ with T presently observed for the primary resonance conforms very well with the behaviour of $\Delta H_{\rm pp}(T)$ usually found in amorphous ferromagnets which exhibit re-entrant spin-glass behaviour at low temperatures (case (*b*) in figure 1).

Recent bulk magnetization measurements (Kaul 1991) taken in fields up to $H =$ 15 kOe on amorphous alloy samples having the same composition and coming from the same batch as the present one reveal that (i) the observed temperature dependence of magnetization is best described by a combination of $T^{3/2}$ and T^2 power laws (the Bloch $T^{3/2}$ law represents the spin-wave contribution whereas the T^2 dependence arises from the single-particle excitations) and (ii) the values of the spin-wave stiffness coefficient $D = 32 \pm 1$ (29 ± 1) meV Å^2 and the coefficient of T^2 term $A = 1.0 \pm 0.2$ $(1.5 \pm 0.2) \times 10^{-6}$ K^{-2} for a-$Fe_{90}Zr_{10}$ (a-$Fe_{91}Zr_9$) are *field-independent*. The reduced bulk magnetization, $M(H, T)/M(H, 0)$, data taken at $H = 7.5$ kOe (mid-value of the

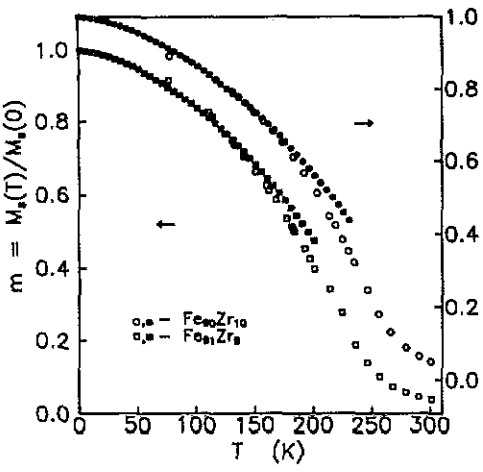

Figure 8. Temperature dependence of $M_s(T)/M_s(0)$, open symbols, and $M(H = 7.5\,\text{kOe}, T)/M(H = 7.5\,\text{kOe}, 0)$, full symbols, for amorphous $Fe_{90}Zr_{10}$ and $Fe_{91}Zr_9$ alloys.

field range covered) with $M(H, 0) = 1010$ G (1000 G) are compared with the reduced saturation magnetization, $M_s(T)/M_s(0)$, data, deduced from the present FMR measurements (main resonance), with $M_s(0) = 903$ G (896 G) in figure 8. A very good agreement between the two sets of data is evident from this figure. Note that $M_s(T)$ can be approximated by a T^2 law alone within the temperature range $77\,\text{K} \leqslant T \leqslant 200\,\text{K}$ for both the alloys and the above values of $M_s(0)$ are deduced from such fits. Another important observation worth noting is that the temperature range over which the two sets of data overlap broadens and $M(H, 0)$ approaches $M_s(0)$ as the bulk magnetization (BM) data taken at lower field values are used for comparison, e.g. for the $M(H = 1\,\text{kOe}, T)/M(H = 1\,\text{kOe}, 0)$ data, $M(H = 1\,\text{kOe}, 0) = 900$ G (894 G) for a-$Fe_{90}Zr_{10}$ (a-$Fe_{91}Zr_9$) and the FMR data conform very well with the BM data for temperatures up to $T \simeq T_C$. For the time being, we ignore the spin-wave contribution and consider only the contribution to thermal demagnetization due to single-particle excitations within the framework of a theory (Wohlfarth 1976), based on the collective (itinerant) electron model, for a weak itinerant ferromagnet, i.e.

$$M_s(T)/M_s(0) = 1 - AT^2 \tag{7}$$

$$= 1 - (2\pi^2 k_B^2 f^2/\mu^2)[N(E_F)]^2 T^2 \tag{8a}$$

with

$$f^2 = \frac{[N'(E_F)/N(E_F)]^2 - [N''(E_F)/N(E_F)]}{3[N'(E_F)/N(E_F)]^2 - [N''(E_F)/N(E_F)]} \tag{8b}$$

where μ is the magnetic moment per alloy atom, $N(E_F)$ is the density of single-particle states at the Fermi level E_F, and $N'(E_F)$ ($N''(E_F)$) is its first (second) energy derivative. A comparison between equations (7) and (8*a*) then yields the following relation between $N(E_F)$ and the coefficient A of the T^2 term

$$N(E_F) = (\mu/\pi k_B f)(A/2)^{1/2}. \tag{9}$$

Equation (9) permits a calculation of $N(E_F)$ provided the exact value of the function f is known. This requires complete knowledge about the actual shape of the density-of-states curve (equation (8*b*)) which is lacking at present for the alloys in question.

However, ultraviolet and x-ray photoelectron emission spectroscopic studies (Guntherodt *et al* 1980, Amamou 1980, Oelhafen *et al* 1980, Onn *et al* 1983, Tenhover and Johnson 1983, Tenhover *et al* 1984) on Zr-rich (Fe, Co)-Zr amorphous alloys show that the Fermi level lies fairly close to the top of the Zr 4d band. If we assume that E_F for the investigated alloys lies close to the top of the (Fe, Co) 3d band and 3d bands are Gaussian-like in shape, $f \simeq 1$. Setting $f = 1$ and using the experimentally determined (Kaul 1991) values of the coeficient A and μ in equation (9) yields the values for the density of states at E_F as $N(E_F) = 3.4 \pm 0.1$ states/eV atom and 4.0 ± 0.1 states/eV atom for amorphous $Fe_{90}Zr_{10}$ and $Fe_{91}Zr_9$ alloys, respectively. These values compare favourably with those determined from the low-temperature specific-heat measurements (Mizutani *et al* 1984), i.e. $N(E_F) = 4.4$ states/eV atom (4.7 states/eV atom) for a-$Fe_{90}Zr_{10}$ (a-$Fe_{91}Zr_9$), after making corrections for the electron–electron and electron–phonon enhancement (Batalla *et al* 1985) and also with the estimate of 2.0 states/eV atom for Fe_3Zr compound based on the band-structure calculations of Malozemoff *et al* (1983). From the finding that a large value of the coefficient A of the T^2 term, *characteristic* (Nakai *et al* 1983) of invar systems, is responsible for a close agreement between magnetization and specific-heat results we conclude that a major contribution to the term linear in T in the low-temperature specific heat for a-$Fe_{90\pm x}Zr_{10\mp x}$ alloys is due to the invar effect or equivalently due to weak ferromagnetism.

In order to facilitate a discussion of the FMR results presented in figures 2–6 in terms of the physical pictures proposed hitherto in the literature to understand the type of magnetism in amorphous $Fe_{90\pm x}Zr_{10\mp x}$ alloys, we recall the main findings of the present investigation, namely, (i) a primary resonance, characterized by a *finite* anisotropy field, H_k, which scales with saturation magnetization, and a temperature dependence of the peak-to-peak linewidth reminiscent of that usually found in re-entrant spin-glass systems (figure 1(*b*)), persists to temperatures as high as $1.5T_C$, and (ii) a secondary resonance, characterized by $H_k = 0$, large M_s and a variation of $\Delta H'_{pp}$ with T similar to that observed in cluster spin glasses (figure 1(*c*)) (but this resonance in the amorphous alloys in question, unlike the one in cluster spin-glass materials, is much sharper and symmetrical with respect to the baseline), is observed only for $T > T_C$. In view of the widely different properties of the two resonances and the fact that the secondary resonance can be observed *only* for temperatures *well above* T_C, the possibility of interpreting these resonances as arising from regions of the sample that differ slightly in composition is completely ruled out. Moreover, the model descriptions like the 'wandering-axis' ferromagnet (Ryan *et al* 1987, Coey *et al* 1987) and a strongly exchange-frustrated spin system with short-ranged (Fish and Rhyne 1987) ferromagnetic correlations, by definition, preclude development of a long-range ferromagnetic order at any temperature and hence can at best qualitatively explain certain features of the secondary resonance, i.e. $H_k \simeq 0$ and $\Delta H'_{pp}(T)$, but certainly not the occurrence of this resonance only for temperatures above a certain temperature, T_C, and the existence of another (main) resonance with properties characteristic of long-range ferromagnetic order. Now that the diverse aspects of Mössbauer data (Kaul *et al* 1988, Siruguri *et al* 1991), spin-wave excitations (Kaul 1991) and critical behaviour near the FM–PM phase transition (Kaul *et al* 1986, Kaul 1987, 1988) in a-$Fe_{90\pm x}Zr_{10\mp x}$ alloys find a simple but coherent interpretation in terms of the *infinite* three-dimensional (3D) ferromagnetic network (matrix) plus *finite* spin clusters picture, an attempt is made to find out whether or not this model can provide a plausible explanation for the present results too. Within the framework of this picture, the primary and secondary resonances could occur when the frequency of the microwave field coincides respectively with the frequency of the Larmor

precession of spins constituting the 3D FM matrix and with that of the *coherent* precession of spins within the finite spin clusters around the external static magnetic field (H) direction, as explained below. For temperatures well below T_C, *local* anisotropy fields are expected to be as large as (Elsässer *et al* 1988, Bohm *et al* 1989, Kronmüller 1985) 100 kOe or even larger particularly in the immediate vicinity of the interface (frustration zones) between the 3D FM matrix and finite spin clusters, so that within the external magnetic field range covered in the present experiments, H can hardly affect the orientation of these clusters and hence they do not participate in the resonance process (note that $H_{res} \leqslant 2$ kOe for $T \leqslant T_C$). By contrast, the spins in the 3D FM network respond to the field and give rise to a resonance whose temperature dependence and other properties, i.e. $H_k \propto M_s$, $\lambda \propto M_s$, etc, are characteristic of crystalline and amorphous 3D ferromagnets. However, as T is increased above T_C where *local* anisotropy fields are small, the frustration zones (which survive so long as the net exchange interaction that the spins within these zones experience due to the rest of the spins distributed in the finite clusters and in the FM network is zero) start 'melting' away because the increased randomness in the spin arrangement of the FM matrix caused by thermal agitation weakens the exchange interaction outside whereas the direct exchange interaction between the spins within the finite clusters is strong enough to polarize the spins (some of the spins) originally belonging to the frustration zones (FM matrix) and two or more neighbouring clusters coalesce to form a bigger cluster. Consequently, the finite clusters grow in size and their relaxation rate decreases. Such clusters are exposed to the external field, which bodily orients the clusters along its own direction and hence *induces* ferromagnetic interaction between them, and the spins constituting these clusters start precessing around H. In the presence of a field, the relaxation rate of the clusters is thus further reduced and as such the secondary resonance sharpens as temperature increases. But beyond a certain temperature ($\simeq$410 K), the clusters start shrinking in size because the ferromagnetic exchange coupling between the spins within the clusters is now weak enough for the clusters to disintegrate into smaller clusters and individual spins and, as a result, the resonance starts broadening. In this context, it is worth mentioning that the bulk magnetization measurements (Kaul 1988, Reisser *et al* 1988) also indicate the presence of strongly interacting giant 'superparamagnetic-like' clusters at temperatures well above T_C. In the case of a-$Fe_{91}Zr_9$, $T \simeq 450$ K marks the onset of nucleation (irreversible atomic ordering process) and both H'_{res} and $\Delta H'_{pp}$ decrease with increasing temperature. (We did not, however, detect any crystalline regions in the electron micrographs taken at room temperature on samples which had been cycled to 500 K, even though the relaxation effects were evident in spectra taken for $T \geqslant 400$ K in that the location and sharpness of the secondary resonance depended on the duration of time for which the sample was at a particular temperature.) Thus the secondary resonance is observed only for $T \geqslant T_C$. While the shape and stress anisotropies decide the 'easy' direction of magnetization in the FM matrix for $T \leqslant T_C$, the easy direction of magnetization for the finite spin clusters for $T > T_C$ lies *always* along the external magnetic field direction owing to the fact that the field H bodily orients these clusters along its own direction. As a result, the primary resonance is associated with a uniaxial 'in-plane' anisotropy field, H_k, of appreciable strength for temperatures well below T_C whereas $H_k = 0$ for the secondary resonance. In view of the foregoing remarks, weak itinerant electron ferromagnetism and invar effect are inherent properties of the FM matrix, and a major contribution to the term linear in T in the low-temperature specific heat for a-$Fe_{90\pm x}Zr_{10\mp x}$ alloys is due to the invar behaviour (FM matrix). Note that in these alloys the ferromagnetic state gives way to a *mixed state* (Kaul *et al* 1988), in which both

ferromagnetic and cluster spin-glass states *coexist* with one another at low temperatures. In a-$Co_{90}Zr_{10}$, however, the finite spin clusters are few in number and are completely isolated from the 3D FM matrix by the frustration zones so that the cluster spin-glass behaviour does not set in at low temperatures but instead ferromagnetic behaviour persists down to the lowest temperature. It should be emphasized at this stage that the above interpretation of the present data in terms of the clusters plus FM matrix picture is not entirely free from speculation. Clearly more data, obtained through complementary techniques on the same samples as the present ones, are needed to test the validity of the conjectures involved. In this context, the inference drawn from the recent high-resolution small-angle neutron scattering studies (Rhyne *et al* 1988) on a-$Fe_{90+x}Zr_{10-x}$ alloys that two types of spin clusters (those which are typically 200–400 Å in size, presumably static and persist to temperatures well beyond the bulk Curie temperature, T_C, and those which disintegrate at T_C and are responsible for a steep increase in the spin–spin correlation length as T_C is approached on either side) coexist in these non-crystalline materials lends further support to the foregoing arguments.

5. Summary and conclusions

Ferromagnetic resonance (FMR) measurements have been performed on amorphous (a-) $Fe_{90+x}Zr_{10-x}$ alloys with $x = 0$ and 1, and on a-$Co_{90}Zr_{10}$ in the horizontal–parallel, vertical–parallel and horizontal–perpendicular sample configurations at a fixed microwave frequency of $\simeq$9.25 GHz in the temperature range 77 to 500 K. The results obtained and the conclusions drawn from them are summarized as follows.

(i) The temperature dependence observed for the resonance fields in the horizontal–parallel ($\|^h$) and vertical–parallel ($\|^v$) sample geometries in the case of the primary resonance for a-$Fe_{90}Zr_{10}$ and a-$Fe_{91}Zr_9$ and for a-$Co_{90}Zr_{10}$ yields the result that $H_k \propto M_s$ for $T \lesssim T_C$. This result is taken to imply that the anisotropy energy is of dipolar origin.

(ii) The property of a-$Fe_{90\pm x}Zr_{10\mp x}$ alloys that the Gilbert damping parameter scales with M_s, characteristic of a large number of crystalline and amorphous ferromagnetic materials, strongly suggests that a long-range ferromagnetic ordering exists in these alloys for $T \lesssim T_C$.

(iii) In conformity with results of our earlier bulk magnetization studies (Kaul 1983, 1991) on samples from the same batch as the present one, the FMR data reveal that both the Stoner single-particle and spin-wave excitations contribute to the thermal demagnetization and a large single-particle contribution leads to an enhancement of the term linear in T in the low-temperature specific heat for the Fe-rich Fe–Zr glassy alloys, and that a-$Co_{90}Zr_{10}$ exhibits a behaviour typical of normal ferromagnets with a very high Curie temperature.

(iv) All the diverse aspects of the FMR data, i.e. the findings (i)–(iii) above, the existence of only a single (primary) resonance for $T \lesssim T_C$ and two resonances (primary and secondary) for $T > T_C$, and $H_k = 0$ for the secondary resonance even though M_s has a considerably large value, find a tentative explanation in terms of the *finite* spin clusters plus an *infinite* 3D ferromagnetic matrix picture.

Acknowledgments

The authors are grateful to Dr M Fähnle, Max-Planck-Institut für Metallforschung, Stuttgart, Germany, for providing the amorphous $Fe_{91}Zr_9$ alloy sample. One of us (VS)

gratefully acknowledges the financial assistance extended to him by the Council of Scientific and Industrial Research, India, in the form of a Senior Research Fellowship.

Appendix

In this section, we briefly outline the calculations leading to equations (2)–(4) and (6) of the text.

Consider an ellipsoidal isotropic ferromagnetic sample which is subjected to a homogeneous external static magnetic field $\boldsymbol{H}$ directed along the z axis and to a weak alternating magnetic field, $\boldsymbol{h}(t) = \boldsymbol{h}\,e^{i\omega t}$ ($|\boldsymbol{h}(t)| \ll |\boldsymbol{H}|$) acting in the xy plane. As a result of the combined action of these fields, the magnetization comprises a steady and an alternating component, i.e. $\boldsymbol{M} = \boldsymbol{M}_s + \boldsymbol{m}(t)$ with $\boldsymbol{m}(t) = \boldsymbol{m}\,e^{i\omega t}$ and $|\boldsymbol{m}(t)| \ll |\boldsymbol{M}_s|$. Assuming that the steady field is intense enough to saturate the ferromagnetic sample so that $\boldsymbol{M}_s$ and $\boldsymbol{H}$ point in the same direction, the Landau–Lifshitz–Gilbert (LLG) phenomenological equation of motion for magnetization is

$$d\boldsymbol{M}/dt = -\gamma(\boldsymbol{M} \times \boldsymbol{H}_{eff}) + (\lambda/\gamma M^2)(\boldsymbol{M} \times d\boldsymbol{M}/dt). \tag{A1}$$

In this equation, the first term is the torque experienced by the magnetization vector and the second term is the damping term of Gilbert form, $\boldsymbol{H}_{eff} = \boldsymbol{H} + \boldsymbol{h}(t) - \boldsymbol{H}_{dem} + \boldsymbol{H}_k$, where $\boldsymbol{H}_{dem} = \boldsymbol{D} \cdot \boldsymbol{M}$ and $\boldsymbol{H}_k = -\boldsymbol{D}_k \cdot \boldsymbol{M}$ denote the demagnetizing field and the uniaxial anisotropy field (with easy axis along $\boldsymbol{H}$), respectively, $\boldsymbol{D}$ and $\boldsymbol{D}_k$ are diagonal tensors, $\gamma = g|e|/2mc$ is the magnetomechanical ratio, M_s is the saturation magnetization and λ is the Gilbert damping parameter.

Substitution for $\boldsymbol{M}$ and $\boldsymbol{H}_{eff}$ in equation (A1) yields

$$\begin{aligned} d\boldsymbol{m}(t)/dt = &-\gamma[\boldsymbol{M}_s \times \boldsymbol{h}(t) + \boldsymbol{m}(t) \times \boldsymbol{H} - \boldsymbol{M} \times (\boldsymbol{D} \cdot \boldsymbol{M}) - \boldsymbol{M} \times (\boldsymbol{D}_k \cdot \boldsymbol{M})] \\ &+ (\lambda/\gamma M^2)([\boldsymbol{M}_s + \boldsymbol{m}(t)] \times (d/dt)[\boldsymbol{M}_s + \boldsymbol{m}(t)]) \end{aligned} \tag{A2}$$

where use has been made of the relation $d\boldsymbol{M}_s/dt = 0 = -\gamma(\boldsymbol{M}_s \times \boldsymbol{H})$ and the term $-\gamma[\boldsymbol{m}(t) \times \boldsymbol{h}(t)]$ has been dropped because of its small magnitude. Using the above-mentioned exponential variation of $\boldsymbol{m}$ with time and neglecting the second-order terms, the Cartesian components of (A2) can finally be written in the form

$$(i\omega/\gamma)m_x + [H + (D_y + D_{ky} - D_z - D_{kz})M_s + i\Gamma]m_y = M_s h_y \tag{A3}$$

$$-[H + (D_x + D_{kx} - D_z - D_{kz})M_s + i\Gamma]m_x + (i\omega/\gamma)m_y = -M_s h_x \tag{A4}$$

and

$$m_z = 0 \tag{A5}$$

where $\Gamma = \lambda\omega/\gamma^2 M_s$. Elimination of m_y from equations (A3) and (A4) gives

$$m_x = \chi_{xx} h_x + \chi_{xy} h_y \tag{A6}$$

with

$$\chi_{xx} = [H + (D_y + D_{ky} - D_z - D_{kz})M_s + i\Gamma]M_s \eta^{-1} \tag{A7}$$

$$\chi_{xy} = (i\omega/\gamma)M_s \eta^{-1} \tag{A8}$$

and

$$\eta=[H+(D_x+D_{kx}-D_z-D_{kz})M_s][H+(D_y+D_{ky}-D_z-D_{kz})M_s]-\Gamma^2-(\omega/\gamma)^2 + i\Gamma[2H+(D_x+D_y+D_{kx}+D_{ky}-2D_z-2D_{kz})M_s]. \tag{A9}$$

If we had eliminated m_x instead of m_y from equations (A3) and (A4), we would have obtained the result

$$m_y = \chi_{yx}h_x + \chi_{yy}h_y \tag{A10}$$

where $\chi_{xx}=\chi_{yy}=\chi$ is the dynamic susceptibility and $\chi_{xy}=-\chi_{yx}=iG$, G is the gyration vector. Recalling that both the dynamic susceptibility χ and dynamic permeability μ are complex, i.e. $\chi=\chi'-i\chi''$ and $\mu=\mu'-i\mu''$, and using the relation $\mu=1+4\pi\chi$, the real and imaginary components of the (complex) dynamic permeability are given by

$$\mu'=[[\alpha\{[H+(D_y+D_{ky}-D_z-D_{kz})M_s][B+(D_x+D_{kx}-D_z-D_{kz})]-\Gamma^2-(\omega/\gamma)^2\} + \beta\Gamma[(B+H)+(D_x+D_y+D_{kx}+D_{ky}-2D_z-2D_{kz})M_s]]]/(\alpha^2+\beta^2) \tag{A11}$$

$$\mu''=\{-\alpha\Gamma[(B+H_k)-(H+H_k)]+\beta[(B+H_k) - (H+H_k)][H+(D_y+D_{ky}-D_z-D_{kz})M_s]\}/(\alpha^2+\beta^2) \tag{A12}$$

with

$$\alpha=[H+(D_x+D_{kx}-D_z-D_{kz})M_s][H+(D_y+D_{ky}-D_z-D_{kz})M_s]-\Gamma^2-(\omega/\gamma)^2 \tag{A13}$$

$$\beta=\Gamma[2H+(D_x+D_y+D_{kx}+D_{ky}-2D_z-2D_{kz})M_s] \tag{A14}$$

and

$$B=H+4\pi M_s. \tag{A15}$$

For a flat plate (the sample shape used in the present experiments), with H applied along the symmetry axis (z axis) so far as the uniaxial anisotropy is concerned and lying in the sample plane (parallel geometry or configuration), $D_x=D_z=0$, $D_y=4\pi$ (x axis is taken to coincide with the polar axis), $D_{kx}M_s=D_{ky}M_s=H_k$ and $D_{kz}=0$. In this case, equations (A11) and (A12) together with equations (A13) and (A14) reduce to equations (2*a*) and (2*b*) of the text, respectively.

Returning back to equations (A3) and (A4), the resonance frequency $\omega=\omega_{res}$ is given by the condition that m_x and m_y have non-trivial solutions when $h_x=h_y=0$. Alternatively, this condition implies that

$$\begin{vmatrix} i\omega_{res}/\gamma & [H_{res}+(D_y+D_{ky}-D_z-D_{kz})M_s+i\Gamma] \\ -[H_{res}+(D_x+D_{kx}-D_z-D_{kz})M_s+i\Gamma] & i\omega_{res}/\gamma \end{vmatrix}=0$$

where H_{res} is the steady field corresponding to ω_{res}. After a few simplifying steps, we finally obtain

$$[(\omega/\gamma)^2+\Gamma^2]=[H_{res}+(D_y+D_{ky}-D_z-D_{kz})M_s] \times [H_{res}+(D_x+D_{kx}-D_z-D_{kz})M_s]. \tag{A16}$$

Note that the subscript 'res' in ω_{res} has been dropped because in the present FMR experiments the microwave field frequency, ω, is kept constant while the steady field, H, is swept through the resonance.

In the horizontal–parallel ($\|^h$) configuration, H is directed along the z axis (the ribbon length and also the symmetry axis) in the sample (thin ribbon) plane, which also contains the x axis. Hence, $D_x = D_z = 0$, $D_y = 4\pi$, $D_{kx}M_s = D_{ky}M_s = H_k$ and $D_{kz} = 0$, and equation (A16) reduces to

$$[(\omega/\gamma)^2 + \Gamma_{\|h}^2] = (H_{res}^{\|h} + 4\pi M_s + H_k)(H_{res}^{\|h} + H_k). \tag{A17}$$

Since in the vertical–parallel ($\|^v$) configuration, both H and the symmetry axis lie in the ribbon plane and point in the z direction (perpendicular to the ribbon axis) and x direction, respectively, $D_x = D_z = 0$, $D_y = 4\pi$, $D_{ky}M_s = D_{kz}M_s = H_k$ and $D_{kx} = 0$. These values when substituted in equation (A16) yield

$$[(\omega/\gamma)^2 + \Gamma_{\|v}^2] = (H_{res}^{\|v} + 4\pi M_s)(H_{res}^{\|v} - H_k). \tag{A18}$$

In order that equation (A18) has a form similar to that of equation (A17) and is consistent with equation (3*b*) of the text, we assume that $H_k \ll 4\pi M_s$ and put equation (A18) in the desired form, i.e.

$$[(\omega/\gamma)^2 + \Gamma_{\|v}^2] \simeq (H_{res}^{\|v} + 4\pi M_s - H_k)(H_{res}^{\|v} - H_k). \tag{A19}$$

(It will be shown in the concluding part of this section that the condition $H_k \ll 4\pi M_s$, which holds for amorphous ferromagnetic alloys in general, is actually satisfied in the presently investigated glassy systems.) Since the linewidth parameter Γ is independent of H_k and ω is kept fixed in the present experiments, the left-hand side of equations (A17) and (A19) has the same value regardless of the magnitude of H_k. Setting $H_k = 0$ in these equations, therefore, yields

$$(H_{res}^{\|} + 4\pi M_s)H_{res}^{\|} = (H_{res}^{\|h} + 4\pi M_s + H_k)(H_{res}^{\|h} + H_k) \tag{A20}$$

and

$$(H_{res}^{\|} + 4\pi M_s)H_{res}^{\|} \simeq (H_{res}^{\|v} + 4\pi M_s - H_k)(H_{res}^{\|v} - H_k) \tag{A21}$$

where $H_{res}^{\|}$ in the resonance field in the absence of H_k.

It immediately follows that these equations are identically satisfied only when

$$H_{res}^{\|} = H_{res}^{\|h} + H_k \qquad \text{or} \qquad H_{res}^{\|h} = H_{res}^{\|} - H_k \tag{A22}$$

and

$$H_{res}^{\|} \simeq H_{res}^{\|v} - H_k \qquad \text{or} \qquad H_{res}^{\|v} \simeq H_{res}^{\|} + H_k. \tag{A23}$$

Another sample configuration of interest is the horizontal–perpendicular ($\perp^h$) geometry in which H points in the z direction and is normal to the sample plane, which contains both x and y (symmetry axis) axes. In this case, $D_x = D_y = 0$, $D_z = 4\pi$, $D_{kz}M_s = D_{kx}M_s = H_k$ and $D_{ky} = 0$ so that equation (A16) assumes the form

$$[(\omega/\gamma)^2 + \Gamma_{\perp h}^2] = (H_{res}^{\perp h} - 4\pi M_s - H_k)(H_{res}^{\perp h} - 4\pi M_s). \tag{A24}$$

With a view to test the validity of the assumption $H_k \ll 4\pi M_s$ and hence to ascertain whether or not the use of equations (A22) and (A23) to determine H_k is permitted, magnetization (M) of the samples used in the present FMR study was measured as a function of the external static magnetic field (H) in fields up to 18 kOe at various fixed temperature values in the range 77 K to $T = T_C$ along the easy (length, 'l') and hard (breadth, 'b') directions in the ribbon plane using the vibrating sample magnetometer. Values of H_k at different temperatures were then deduced from the difference in the

areas enclosed by the M versus H isotherms (taken along 'b' and 'l'), the ordinate and the line $M = M_s$ with the aid of the relation

$$W_b - W_l = \left[\int_0^{M_s} H\,dM\right]_b - \left[\int_0^{M_s} H\,dM\right]_l = K_u = H_k M_s/2 \qquad \text{(A25)}$$

where W_b and W_l stand for the work done by the field to magnetize the sample along the breadth (hard direction) and length (easy direction), respectively. The results of this investigation demonstrate that H_k is *at least two orders of magnitude smaller* than $4\pi M_s$ at all temperatures within the investigated temperature range and that the values of H_k deduced from the magnetization measurements using equation (A25) are in excellent agreement with the corresponding values estimated from the FMR data employing equations (A22) and (A23). For instance, the bulk magnetization measurements yield the values for H_k ($4\pi M_s$) at 77 K for a-$Co_{90}Zr_{10}$, a-$Fe_{90}Zr_{10}$ and a-$Fe_{91}Zr_9$ alloys as 40 ± 5 Oe (12.95 kG), 85 ± 5 Oe (11.05 kG) and 55 ± 5 Oe (11.55 kG), respectively. These values of H_k should be compared with the corresponding numerical estimates 43 ± 3 Oe, 90 ± 5 Oe and 60 ± 5 Oe obtained from the FMR data.

References

Amamou A 1980 *Solid State Commun.* **33** 1029
Batalla E, Altounian Z and Ström-Olsen J O 1985 *Phys. Rev.* B **31** 577
Beck W and Kronmüller H 1985 *Phys. Status Solidi* b **132** 449
Bhagat S M, Haraldson S and Beckman O 1977 *J. Phys. Chem. Solids* **38** 593
Bhagat S M, Webb D J and Manheimer M A 1985 *J. Magn. Magn. Mater.* **53** 209
Böhm M C, Elsässer C, Fähnle M and Brandt E H 1989 *Chem. Phys.* **130** 65
Cochrane J F, Qiao R W and Heinrich B 1989 *Phys. Rev.* B **39** 4399
Coey J M D, Ryan D H and Buder R 1987 *Phys. Rev. Lett.* **58** 385
Elsässer C, Fähnle M, Brandt E H and Böhm M C 1988 *J. Phys. F: Met. Phys.* **18** 2463
Fish G E and Rhyne J J 1987 *J. Appl. Phys.* **61** 454
Fujimori H 1983 *Amorphous Metallic Alloys* ed F E Luborsky (London: Butterworths) p 300
Ghafari M, Keune W, Brand R A, Day R K and Dunlop J B 1988 *Mater. Sci. Eng.* **99** 65
Guntherodt H J *et al* 1980 *J. Physique Coll.* **41** C8 381
Hasegawa R 1975 *Proc. 21st Ann. Conf. on Magnetism and Magnetic Materials* ed J J Becker, G H Lander and J J Rhyne (New York: AIP) p 216
—— 1983 *Glassy Metals: Magnetic, Chemical and Structural Properties* ed R Hasegawa (Boca Raton, FL: CRC)
Hasegawa R, O'Handley R C and Mendelsohn L T 1976 *Magnetism and Magnetic Materials 1976: Proc. 1st Joint MMM–Intermag. Conf.* ed J J Becker and G H Lander (New York: AIP) p 298
Heinrich B, Cochran J F and Hasegawa R 1985 *J. Appl. Phys.* **57** 3690
Heinrich B, Rudd J M, Urquhart K, Myrtle K, Cochran J F and Hasegawa R 1984 *J. Appl. Phys.* **55** 1814
Heller J A, Wasserman E F, Braun M F and Brand R A 1986 *J. Magn. Magn. Mater.* **54–57** 307
Hiroyoshi H and Fukamichi K 1982 *J. Appl. Phys.* **53** 2226
Kaul S N 1983 *Phys. Rev.* B **27** 6923
—— 1984 *IEEE Trans. Magn.* **MAG-20** 1290
—— 1985 *J. Magn. Magn. Mater.* **53** 5
—— 1987 *J. Appl. Phys.* **61** 451
—— 1988 *J. Phys. F: Met. Phys.* **18** 2089
—— 1991 *J. Phys.: Condens. Matter* **3** 4027
Kaul S N, Bansal C, Kumaran T and Havalgi M 1988 *Phys. Rev.* B **38** 9248
Kaul S N, Hoffman A and Kronmüller H 1986 *J. Phys. F: Met. Phys.* **16** 365
Kaul S N, Mohan Ch V, Babu P D, Sambasiva Rao M and Lucinski T 1991 unpublished results
Kaul S N and Mohan Babu T V S M 1989 *J. Phys.: Condens. Matter* **1** 8509
Kaul S N and Siruguri V 1987 *J. Phys. F: Met. Phys.* **17** L255

Kaul S N and Srinivasa Kasyapa V 1989 *J. Mater. Sci.* **24** 3337
Kraus L, Frait Z and Schneider J 1981 *Phys. Status Solidi* a **63** 669
Kronmüller H 1985 *Phys. Status Solidi* b **127** 531
Luborsky F E 1980 *Ferromagnetic Materials* ed E P Wolhlfarth (Amsterdam: North-Holland) vol 1, p 451
Luborsky F E and Walter J L 1977 *IEEE Trans. Magn.* **MAG-13** 1635
Malozemoff A P, Williams A R, Terakura K, Moruzzi V L and Fukamichi K 1983 *J. Magn. Magn. Mater.* **35** 192
Mizutani U, Matsuura M and Fukamichi K 1984 *J. Phys. F: Met. Phys.* **14** 731
Mohan Babu T V S M 1988 *MPhil Thesis* University of Hyderabad (unpublished)
Nakai I, Ono F and Yamada O 1983 *J. Phys. Soc. Japan* **52** 1791
Oelhafen P, Hauser E and Guntherodt H J 1980 *Solid State Commun.* **35** 1017
Onn D G, Wang L Q and Fukamichi K 1983 *Solid State Commun.* **47** 479
Oshima R, Tanimoto M, Fujita E F, Nose M and Masumoto T 1981 *Proc. 4th Int. Conf. on Rapidly Quenched Metals* ed T Masumoto and K Suzuki (Sendai: Institute of Metals) vol II, p 117
Park M J, Bhagat S M, Manheimer M A and Moorjani K 1986 *J. Magn. Magn. Mater.* **59** 287
Read D A, Moyo T and Hallam G C 1986 *J. Magn. Magn. Mater.* **54–57** 309
Reisser R, Fähnle M and Kronmüller H 1988 *J. Magn. Magn. Mater.* **75** 45
Rhyne J J, Erwin R W, Fernandez-Baca J A and Fish G E 1988 *J. Appl. Phys.* **63** 4080
Rhyne J J and Fish G E 1985 *J. Appl. Phys.* **57** 3407
Ryan D H, Coey J M D, Batalla E, Altounian Z and Strom-Olsen J O 1987 *Phys. Rev.* B **35** 8630
Saito N, Hiroyoshi H, Fukamichi K and Nakagawa Y 1986 *J. Phys. F: Met. Phys.* **16** 911
Siruguri V, Kaul S N, Rajaram G and Chandra G 1991 *Anal. Fis.* B **86** 181
Siruguri V, Mohan Ch V and Kaul S N 1991 unpublished results
Takahashi M and Kim C O 1978 *Japan J. Appl. Phys.* **16** 206
Tange H, Inoue K and Shirakawa K 1986 *J. Magn. Magn. Mater.* **54–57** 303
Tenhover M and Johnson W L 1983 *Phys. Rev.* B **27** 1610
Tenhover M, Lucko D and Suran D 1984 *Phys. Rev.* B **29** 2306
Winschuh K and Rosenberg M 1987 *J. Appl. Phys.* **61** 4401
Wohlfarth E P 1976 *Magnetism: Selected Topics* ed S Foner (New York: Gordon and Breach) p 59
Yamamoto H, Onodera H, Hosoyama K, Masumoto T and Yamauchi H 1983 *J. Magn. Magn. Mater.* **31–34** 1579
Yamauchi H, Onodera H and Yamamoto H 1984 *J. Phys. Soc. Japan* **53** 747